IEEE Access
Multidisciplinary | Rapid Review | Open Access Journal

Received March 4, 2019, accepted April 1, 2019, date of publication April 9, 2019, date of current version April 18, 2019.

Digital Object Identifier 10.1109/ACCESS.2019.2909657

Dynamic Modeling, Simulation, and Experimental Verification of a Wafer Handling SCARA Robot With Decoupling Servo Control

YUNBO HE, XIQUAN MAI, CHENGQIANG CUI, JIAN GAO, ZHIJUN YANG, KAI ZHANG, XUN CHEN, YUN CHEN, AND HUI TANG
Guangdong University of Technology, Guangzhou 510006, China

Corresponding author: Xiquan Mai (maixiquan@foxmail.com)

This work was supported in part by the Guangdong Provincial Natural Science Foundation under Grant 2016A030308016 and Grant 2015A030312008, in part by the R&D Key Projects from Guangdong Province under Grant 2015B010133005, Grant 2015B010104006, and Grant 17ZK0091, and in part by the National Natural Science Foundation under Grant 51675106 and Grant U1601202.

ABSTRACT In this paper, we propose a novel coordinated control method based on decoupling servo control to design a 4-DOF direct-drive SCARA robot for wafer handling purpose. As the basis of decoupling servo control, the dynamic model of the SCARA robot is obtained with two methods, the Newton–Euler equation, and Lagrangian equation. The validity of this SCARA dynamic equation is confirmed by these two methods. Due to disturbance and model uncertainty, three PD plus robust controllers are individually applied to three axes of the SCARA robot, together with decoupling control on three physically dynamically highly coupled robotic arms. The inverse dynamics of the SCARA robot is analyzed by feedback linearization, and the experimental results show that above PD plus robust controllers and decoupling control reduce the position tracking error effectively. Performance meets with the high speed and high precision requirements in the wafer handling process. The experimental data shows that the decoupling control algorithm makes the SCARA robot performance improved a lot. The position errors during dynamic tracking movement and the static errors are reduced by 4 to 20 times.

INDEX TERMS Decoupling control, direct-drive, wafer handling, SCARA robot.

I. INTRODUCTION

With high density integration of integrated circuits, the precision and motion smoothness requirements of wafer handlers are getting stricter and stricter. Wafer handling SCARA robot, an indispensable device in the Integrated Circuits manufacturing, can transfer and align wafers during different working procedures [1]–[4]. Meanwhile, Wafer handling robot is a multi-disciplinary product including machinery, electronics, computer, and in the limited space to achieve the rapid conversion of the wafer station, so an increasing demand for a higher speed, higher reliability, and higher action precision [5].

Several methods have been proposed in the paper related to the design controllers for robot manipulators such as proportional–integral–differential (PID) [6]–[8], sliding mode control [9]–[11], fuzzy logic control [9], [12], [13], adaptive control [14]–[16], neural network [17]–[19], backstepping method [20], [21], artificial intelligence [22], etc. The work of Son *et al.* [23] proposes a control system combining adaptively feed-forward neural controller and PID controller. The adaptively feed-forward neural controller dynamically identifies all nonlinear features using an inverse neural NARX (INN) model. The experimental results of their work have shown the performance and merits of the proposed control method. However, the control algorithm is complicated. The work of Fateh and Fateh [24] proposes a fine-tuning fuzzy control of robots. With this controller, trajectory tracking control simulations and experiments were carried out using an articulated electrically driven robot manipulator. The convergence analysis can robust track target path efficiently. However, the fine-tuning fuzzy control adapts only one fuzzy rule. The work of Rossomando Soria [25] proposes a neural sliding mode dynamic control in the discrete-time domain. The weights of the radial basis functions (RBF)

The associate editor coordinating the review of this manuscript and approving it for publication was Bora Onat.

can be regulated by an online adaptation law. The sliding surface can limit the adaptation law, and the compensation by sliding surface is designed to delete the approximation error introduced by the neuronal controller. However, the neural sliding mode dynamic control theory is not yet integrated, the parameter setting is difficult and the application field is limited. Since the SCARA robot manipulator being composed of several joint bonded together so that the joint have highly nonlinear dynamics with a strong link between them, traditional method is difficult to achieve good dynamic and stability performance.

In recent years, with the development of non-linear control, decoupling servo control has attracted much attention. Decoupling servo control is based on the concept of the nonlinear estimation. Several paper [26]–[28] have been proposed related to decoupling servo control. However, decoupling control has not been applied to robots with 4-DOF direct-drive robot. In this paper, we propose a novel coordinated control method based on decoupling servo control to design a 4-DOF direct-drive SCARA robot is for wafer handling purpose. As the basis of decoupling servo control, the dynamic model of the SCARA robot is obtained with two methods, the Newton-Euler equation and Lagrangian equation. The derivation results of these two methods meet with each other. Due to disturbance and model uncertainty, three PD plus robust controllers are individually applied to three axes of the SCARA robot, together with decoupling control. The inverse dynamics of the SCARA robot is analyzed by feedback linearization, and the experimental results show that above PD plus robust controllers and decoupling control reduce the position tracking error effectively. The experimental data shows, decoupling control algorithm makes SCARA robot performance improved a lot. The position errors during dynamic tracking movement and the static errors are reduced by 4 to 20 times.

This work is organized as in the following way: Section II shows the mathematical representation of the SCARA robot kinematics and dynamics. The feedback decoupling linearization and robust control of the decoupled system are studied in Sects. 3. The simulation models of SCARA robot is shown in Sect. 4. Experimental results are shown in Sect. 5, showing the performance of the controllers. Finally, the conclusions are shown in Sect. 6.

II. THE KINEMATICS AND DYNAMIC MODEL OF SCARA ROBOT

Fig. 2 reflects the structure of the SCARA robot, which has three rotational joints distributed in the X-Y plane and a prismatic joint along the Z-axis (vertical axis) direction. Since the three rotational joints of the direct drive SCARA robot on the XY plane are strongly coupled, this paper focuses on the kinematics and dynamics mode of the three rotational joints. Three rotational arms are called Shoulder, Elbow, Wrist, respectively (see Fig. 1). Based on above definitions and explanations, this paper proposes a direct-drive SCARA robot decoupling control algorithm.

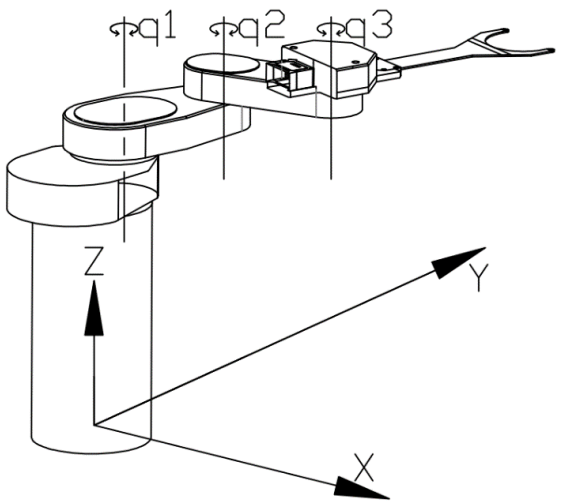

FIGURE 1. SCARA robot manipulator.

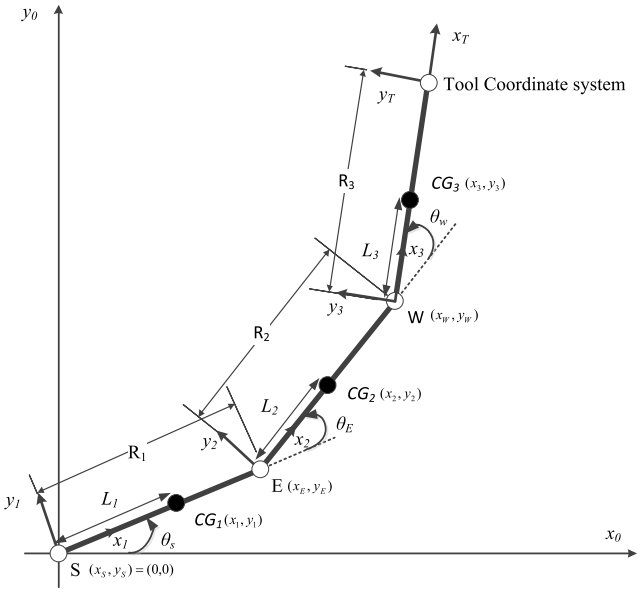

FIGURE 2. Schematic diagram of the SCARA robot.

TABLE 1. D-H parameters of the SCARA robot.

Joint	α_{i-1}	a_{i-1}	d_i	Θ_i
1	0	0	0	Θ_S
2	0	R_1	0	Θ_E
3	0	R_2	0	Θ_W
Tool coordinate system origin	0	R_3	0	0

A. JACOBIAN FOR SCARA ROBOT

Table 1 lists the modified D-H parameters for the SCARA robot and Figure 2 shows the modified D-H coordinate system of each joint, the length of each link and the centroid of each link e Now we use these Link parameters to compute the Jacobian Matrix of the SCARA robot.

Let: $(x_S, y_S) = (0, 0)$

Through the geometrical relationship between the various links, we can get the following equations

$$\begin{aligned} x_E &= R_1 \cos(\theta_S) \\ y_E &= R_1 \sin(\theta_S) \end{aligned} \tag{1}$$

$$\begin{aligned} x_W &= R_2 \cos(\theta_S + \theta_E) + R_1 \cos(\theta_S) \\ y_W &= R_2 \sin(\theta_S + \theta_E) + R_1 \sin(\theta_S) \end{aligned} \tag{2}$$

$$\begin{aligned} x_T &= R_3 \cos(\theta_S + \theta_E + \theta_W) + R_2 \cos(\theta_S + \theta_E) + R_1 \cos(\theta_S) \\ y_T &= R_3 \sin(\theta_S + \theta_E + \theta_W) + R_2 \sin(\theta_S + \theta_E) + R_1 \sin(\theta_S) \end{aligned} \tag{3}$$

By dividing both sides of Eq. (3) by the differential time element, we get the Jacobian

$$\begin{aligned} \dot{x}_T = &[-R_3 \sin(\theta_S + \theta_E + \theta_W) - R_2 \sin(\theta_S + \theta_E) - R_1 \sin(\theta_S)]\dot{\theta}_S \\ &+ [-R_3 \cos(\theta_S + \theta_E + \theta_W) - R_2 \cos(\theta_S + \theta_E)]\dot{\theta}_E \\ &- R_3 \cos(\theta_S + \theta_E + \theta_W)\dot{\theta}_W \end{aligned} \tag{4}$$

$$\begin{aligned} \dot{y}_T = &[R_3 \cos(\theta_S + \theta_E + \theta_W) + R_2 \cos(\theta_S + \theta_E) + R_1 \cos(\theta_S)]\dot{\theta}_S \\ &+ [R_3 \cos(\theta_S + \theta_E + \theta_W) + R_2 \cos(\theta_S + \theta_E)]\dot{\theta}_E \\ &+ R_3 \cos(\theta_S + \theta_E + \theta_W)\dot{\theta}_W \end{aligned} \tag{5}$$

The general form of the Jacobian (In the X-Y plane) is

$$\begin{pmatrix} \dot{x}_T \\ \dot{y}_T \end{pmatrix} = J \begin{pmatrix} \dot{\theta}_S \\ \dot{\theta}_E \\ \dot{\theta}_W \end{pmatrix} \tag{6}$$

From Eq. (6), it's clear that the Jacobian reflects the transformation from joint velocities to Cartesian velocities. The Jacobian written in Eq. (6) is derived from Eq. (4) and Eq. (5) as below

$$J = \begin{bmatrix} -R_3 S_{SEW} - R_2 S_{SE} - R_1 S_S & -R_3 S_{SEW} - R_2 S_{SE} - R_3 S_{SEW} \\ R_3 C_{SEW} + R_2 C_{SE} + R_1 C_S & R_3 C_{SEW} + R_2 C_{SE} R_3 C_{SEW} \end{bmatrix} \tag{7}$$

where S_{SEW} is the abbreviation of $\sin(\theta_S + \theta_E + \theta_W)$, C_{SEW} for $\cos(\theta_S + \theta_E + \theta_W)$, S_{SE} for $\sin(\theta_S + \theta_E)$, C_{SE} for $\cos(\theta_S + \theta_E)$, S_S for $\sin(\theta_S)$, C_S for $\cos(\theta_S)$ and so on. The length of the link R_i, centroid of each link L_i, the angles θ_S, θ_E and θ_W are shown in Fig. 2.

B. DYNAMIC MODEL

In this part, the Newton-Euler equation and the Lagrangian equation are used to obtain the dynamic model of the SCARA robot, respectively.

The Newton-Euler equation is used first. The force relationship between the links of the SCARA robot is shown in Fig. 3. By using force equations (Newton's 2nd law) and moment equations (Euler's law), we can derive the force equations for arms of SCARA robot

$$\begin{pmatrix} f_{Wx} \\ f_{Wy} \end{pmatrix} = \begin{pmatrix} m_3 \ddot{x}_3 \\ m_3 \ddot{y}_3 \end{pmatrix} \tag{8}$$

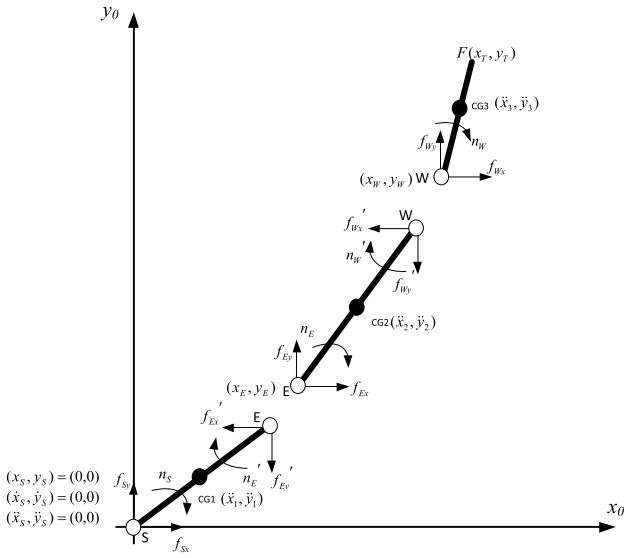

FIGURE 3. The force relationship between the links of the SCARA robot.

$$\begin{pmatrix} f_{Ex} \\ f_{Ey} \end{pmatrix} = \begin{pmatrix} m_2 \ddot{x}_2 + f_{Wx} \\ m_2 \ddot{y}_2 + f_{Wy} \end{pmatrix} = \begin{pmatrix} m_2 \ddot{x}_2 + m_3 \ddot{x}_3 \\ m_2 \ddot{y}_2 + m_3 \ddot{y}_3 \end{pmatrix}] \tag{9}$$

$$\begin{pmatrix} f_{Sx} \\ f_{Sy} \end{pmatrix} = \begin{pmatrix} m_1 \ddot{x}_1 + f_{Ex} \\ m_1 \ddot{y}_1 + f_{Ey} \end{pmatrix} = \begin{pmatrix} m_1 \ddot{x}_1 + m_2 \ddot{x}_2 + m_3 \ddot{x}_3 \\ m_1 \ddot{y}_1 + m_2 \ddot{y}_2 + m_3 \ddot{y}_3 \end{pmatrix} \tag{10}$$

$$n_W = I_3 \dot{\omega}_W - m_3 \ddot{x}_3 (y_3 - y_W) + m_3 \ddot{y}_3 (x_3 - x_W) \tag{11}$$

$$\begin{aligned} n_E = &\, n_W + I_2 \dot{\omega}_E - m_2 \ddot{x}_2 (y_2 - y_E) - m_2 \ddot{y}_2 (x_E - x_2) \\ &+ f_{Wx}(y_W - y_E) + f_{Wy}(x_E - x_W) \end{aligned} \tag{12}$$

$$\begin{aligned} n_S = &\, n_E + I_1 \dot{\omega}_S - m_1 \ddot{x}_1 (y_1 - y_S) + m_1 \ddot{y}_1 (x_1 - x_S) \\ &- f_{Ex}(y_E - y_S) + f_{Ey}(x_E - x_S) \end{aligned} \tag{13}$$

where n_W, n_E, n_S are moment (or force) on three joints of the SCARA robot, and m_i, I_i are the mass and inertia of each link, respectively.

$$\begin{aligned} \omega_S &= \dot{\theta}_S, \quad \dot{\omega}_S = \ddot{\theta}_S \\ \omega_E &= \dot{\theta}_E + \dot{\theta}_S \dot{\omega}_E = \ddot{\theta}_E + \ddot{\theta}_S \\ \omega_W &= \dot{\theta}_S + \dot{\theta}_E + \dot{\theta}_W \dot{\omega}_W = \ddot{\theta}_S + \ddot{\theta}_E + \ddot{\theta}_W \end{aligned}$$

where θ, $\dot{\theta}$, $\ddot{\theta}$ are joint angle, velocities, and accelerations respectively.

Substituting the variables (the acceleration of each centroid, the coordinates of the position of each centroid, the coordinate position of each link) into equations (11), (12), and (13). After simplification, it's shown as below

$$\begin{aligned} n_S = &\, (I_1 + I_2 + I_3 + m_1 L_1^2 + m_2 L_2^2 + m_2 R_1^2 + m_3 L_3^2 + m_3 R_1^2 \\ &+ m_3 R_2^2 + 2 m_3 L_3 R_1 C_{EW} - 2 m_2 L_2 R_1 C_E \\ &- 2 m_3 L_3 R_2 C_W - 2 m_3 R_2 R_1 C_E)\ddot{\theta}_S \\ &+ (I_2 + I_3 + m_2 L_2^2 + m_3 L_3^2 + m_3 R_2^2 + m_3 L_3 R_1 C_{EW} \\ &- m_2 L_2 R_1 C_E - 2 m_3 L_3 R_2 C_W - m_3 R_2 R_1 C_E)\ddot{\theta}_E \\ &+ (I_3 + m_3 L_3^2 + m_3 L_3 R_1 C_{EW} - m_3 L_3 R_2 C_W)\ddot{\theta}_W \\ &+ (-m_3 L_3 R_1 S_{EW} + m_2 L_2 R_1 S_E + m_3 R_2 R_1 S_E)\dot{\theta}_E^2 \end{aligned}$$

$$
\begin{aligned}
&+(-m_3L_3R_1S_{EW}+m_3L_3R_2S_W)\dot{\theta}_W^2\\
&+(-2m_3L_3R_1S_{EW}+2m_2L_2R_1S_E+2m_3R_2R_1S_E)\dot{\theta}_S\dot{\theta}_E\\
&+(-2m_3L_3R_1S_{EW}+2m_3L_3R_2S_W)\dot{\theta}_S\dot{\theta}_W\\
&+(-2m_3L_3R_1S_{EW}+2m_3L_3R_2S_W)\dot{\theta}_E\dot{\theta}_W \qquad (14)\\
n_E &= (I_2+I_3+m_3L_3^2+m_3R_2^2+m_2L_2^2-2m_3L_3R_2C_W\\
&+m_3L_3R_1C_{EW}-m_3R_2R_1C_E-m_2L_2R_1C_E)\ddot{\theta}_S\\
&+(I_2+I_3+m_3L_3^2+m_3R_2^2+m_2L_2^2-2m_3L_3R_2C_W)\ddot{\theta}_E\\
&+(I_3+m_3L_3^2-m_3L_3R_2C_W)\ddot{\theta}_W+(m_3L_3R_1S_{EW}\\
&-m_3R_2R_1S_E-m_2L_2R_1S_E)\dot{\theta}_S^2+m_3L_3R_2S_W\dot{\theta}_W^2\\
&+2m_3L_3R_2S_W\dot{\theta}_S\dot{\theta}_W+2m_3L_3R_2S_W\dot{\theta}_E\dot{\theta}_W \qquad (15)\\
n_W &= (I_3+m_3L_3^2-m_3L_3R_2C_W+m_3L_3R_1C_{EW})\ddot{\theta}_S\\
&+(I_3+m_3L_3^2-m_3L_3R_2C_W)\ddot{\theta}_E+(I_3+m_3L_3^2)\ddot{\theta}_W\\
&+(-m_3L_3R_2S_W+m_3L_3R_1S_{EW})\dot{\theta}_S^2+(-m_3L_3R_2S_W)\dot{\theta}_E^2\\
&+(-2m_3L_3R_2S_W)\dot{\theta}_S\dot{\theta}_E \qquad (16)
\end{aligned}
$$

When the Newton-Euler equations are evaluated symbolically for any manipulator, a dynamic equation is yielded and can be written in the form

$$\tau = M(\theta)\ddot{\theta}+V(\theta,\dot{\theta})\dot{\theta}+G(\theta) \qquad (17)$$

where $M(\theta)$ is the $n\times n$ mass matrix of the robot, $V(\theta,\dot{\theta})$ is an $n\times n$ matrix of centrifugal and Coriolis terms, and $G(\theta)$ is an $n\times 1$ vector of gravity terms, τ is the $n\times 1$ vector of actuator torques.

With Eqs. (14), (15), (16) and (17), the dynamic model of the SCARA robot can be expressed through Eqs. (18) to (36)

$$M=\begin{bmatrix}M_{11}&M_{12}&M_{13}\\M_{21}&M_{22}&M_{23}\\M_{31}&M_{32}&M_{33}\end{bmatrix}\ \mathrm{V}=\begin{bmatrix}V_{11}&V_{12}&V_{13}\\V_{21}&V_{22}&V_{23}\\V_{31}&V_{32}&V_{33}\end{bmatrix} \qquad (18)$$

$$
\begin{aligned}
M_{11} &= (I_1+I_2+I_3)+m_1L_1^2+m_2(L_2^2+R_1^2-2L_2R_1C_E)\\
&+m_3(L_3^2+R_2^2+R_1^2-2L_3R_2C_W\\
&+2L_3R_1C_{EW}-2R_2R_1C_E) \qquad (19)\\
M_{12} &= (I_2+I_3)+m_2(L_2^2-L_2R_1C_E)\\
&+m_3(L_3^2+R_2^2-2L_3R_2C_W+L_3R_1C_{EW}-R_2R_1C_E)C \qquad (20)\\
M_{13} &= I_3+m_3(L_3^2+L_3R_2C_W+L_3R_1C_{EW}) \qquad (21)\\
M_{21} &= (I_2+I_3)+m_2(L_2^2+L_2R_1C_E)\\
&+-m_3(L_3^2+R_2^2+2L_3R_2C_W\\
&+L_3R_1C_{EW}+R_2R_1C_E) \qquad (22)\\
M_{22} &= (I_2+I_3)+m_2L_2^2+m_3(L_3^2+R_2^2+2L_3R_2C_W) \qquad (23)\\
M_{23} &= I_3+m_3(L_3^2+L_3R_2C_W) \qquad (24)\\
M_{31} &= I_3+m_3L_3^2+m_3L_3R_2C_W+m_3L_3R_1C_{EW} \qquad (25)\\
M_{32} &= I_3+m_3L_3^2+m_3L_3R_2C_W \qquad (26)\\
M_{33} &= I_3+m_3L_3^2 \qquad (27)\\
V_{11} &= (2L_3R_1m_3S_{EW}+2L_2R_1m_2S_E+2R_1R_2m_3S_E)\dot{\theta}_E\\
&-(2L_3R_1m_3S_{EW}+2L_3R_2m_3S_W)\dot{\theta}_W \qquad (28)\\
V_{12} &= (-L_3R_1m_3S_{EW}-L_2R_1m_2S_E-R_1R_2m_3S_E)\dot{\theta}_E \qquad (29)\\
V_{13} &= (-2L_3R_1m_3S_{EW}-2L_3R_2m_3S_W)\dot{\theta}_E\\
&+(-L_3R_1m_3S_{EW}-L_3R_2m_3S_W)\dot{\theta}_W \qquad (30)\\
V_{21} &= (L_3R_1m_3S_{EW}+L_2R_1m_2S_E+R_1R_2m_3S_E)\dot{\theta}_S \qquad (31)\\
V_{22} &= -2L_3R_2m_3S_W\theta_W \qquad (32)\\
V_{23} &= -2L_3R_2m_3S_W\dot{\theta}_S-L_3R_2m_3S_W\dot{\theta}_W \qquad (33)\\
V_{31} &= (L_3R_1m_3S_{EW}+L_3R_2m_3S_W)\dot{\theta}_S \qquad (34)\\
V_{32} &= 2L_3R_2m_3S_W\dot{\theta}_S+L_3R_2m_3S_W\dot{\theta}_E \qquad (35)\\
V_{33} &= 0 \qquad (36)
\end{aligned}
$$

As well, the Lagrangian equation is used to obtain the dynamic model of the SCARA robot.

Lagrangian Equation:

$$\frac{d}{dt}\left(\frac{\partial T}{\partial\dot{\vec{q}}_i}\right)-\frac{\partial T}{\partial\vec{q}_i}+\frac{\partial u}{\partial\vec{q}_i}=\tau_i \qquad (37)$$

where, T is kinetic energy, u is potential energy, $\vec{q}_i$ is angle (or displacement), and τ_i is moment (or force) of its DOE [29].

Kinetic energy of planar motion of a rigid object is shown below

$$K=\frac{1}{2}mV^2+\frac{1}{2}I\omega^2 \qquad (38)$$

So, for this 3-arm SCARA

$$
\begin{aligned}
T &= \frac{1}{2}m_1V_1^2+\frac{1}{2}I_1\omega_1^2+\frac{1}{2}m_2V_2^2+\frac{1}{2}I_2\omega_2^2+\frac{1}{2}m_3V_3^2+\frac{1}{2}I_3\omega_3^2\\
&= \frac{1}{2}(m_1L_1^2+I_1)\dot{\theta}_S^2+\frac{1}{2}I_2(\dot{\theta}_S+\dot{\theta}_E)^2+\frac{1}{2}I_3(\dot{\theta}_S+\dot{\theta}_E+\dot{\theta}_W)^2\\
&+\frac{1}{2}m_2V_2^2+\frac{1}{2}m_3V_3^2 \qquad (39)
\end{aligned}
$$

where

$$
\begin{aligned}
V_1^2 &= L_1^2\dot{\theta}_S^2C_S^2+L_1^2\dot{\theta}_S^2S_S^2 \qquad (40)\\
V_2^2 &= L_2^2\dot{\theta}_S^2+2L_2^2\dot{\theta}_S\dot{\theta}_E+L_2^2\dot{\theta}_E^2\\
&+2C_EL_2R_1\dot{\theta}_S^2+2C_EL_2R_1\dot{\theta}_S\dot{\theta}_E+R_1^2\theta_S^2 \qquad (41)\\
V_3^2 &= (R_1\dot{\theta}_SS_S+L_3\dot{\theta}_SS_{SEW}+L_3\dot{\theta}_ES_{SEW}+L_3\dot{\theta}_WS_{SEW}\\
&+R_2\dot{\theta}_ES_{SE})^2+(R_2\dot{\theta}_SC_{SE}+R_2\dot{\theta}_EC_{SE}+L_3\dot{\theta}_SC_{SEW}\\
&+L_3\dot{\theta}_EC_{SEW}+L_3\dot{\theta}_WC_{SEW}) \qquad (42)
\end{aligned}
$$

So, τ_E and τ_S can be obtained similarly.

$$
\begin{aligned}
\tau_W &= \frac{d}{dt}\left(\frac{\partial T}{\partial\dot{\theta}_W}\right)-\frac{\partial T}{\partial\theta_W}\\
&= (I_3+m_3L_3^2+m_3L_3R_2C_W+m_3L_3R_1C_{EW})\ddot{\theta}_S\\
&+(I_3+m_3L_3^2+m_3L_3R_2C_W)\ddot{\theta}_E+(I_3+m_3L_3^2)\ddot{\theta}_W\\
&+(m_3L_3R_1S_{EW}+m_3L_3R_2S_W)\dot{\theta}_S^2\\
&+m_3L_3R_2S_W\dot{\theta}_E^2+2m_3L_3R_2S_W\dot{\theta}_S\dot{\theta}_E \qquad (43)
\end{aligned}
$$

where τ_S, τ_E, τ_W are the actuator torques of Shoulder, Elbow, Wrist, respectively. By comparing the equations and results from above two methods, we have the equations below

$$n_S=\tau_Sn_E=\tau_En_W=\tau_W \qquad (44)$$

Above equations show the two methods validate each other and verify the correctness of this dynamic equation

of SCARA robot. Since the decoupling control algorithm focuses on three rotational joints (only the X-Y plane motion) of the SCARA robot, the vector of gravity terms becomes zero as below

$$G(\theta) = 0 \tag{45}$$

III. SERVO AND DECOUPLING CONTROLLERS

The PID controller is a simple feedback structure for present-past-future, which does not depend on the precise mathematical models of the dynamical systems to be controlled [30]. So, PD controller is one of the most widely used controllers in the field of industrial robots. Due to mechanical system disturbance and model uncertainty, if Only the PD controller is used, the performance of the robot cannot be met. Therefore, the robust control theory is used to design of the SCARA robot controllers. Since three rotational joints of the direct drive SCARA robot on the X-Y plane are strongly coupled and Feedback linearization scheme can realize decoupling linearization of the mechanical dynamic system, it is a good way to use the PD control together with robust control and the feedback decoupling linearization scheme. The decoupling principle of this control algorithm is analyzed in Section A.

A. FEEDBACK DECOUPLING LINEARIZATION

The basic idea behind the feedback linearization is to design a nonlinear controller that linearizes the nonlinear system by an appropriate state space coordinate change. A second-stage control law can then be designed in the current coordinates to fulfill the main requirements of control, such as decoupling, against disturbances, and model uncertainties [31]. Combined with the previously discussed Eq. (17), the control law u is written as

$$u = \ddot{\theta} = M(\theta)^{-1}(\tau - V(\theta, \dot{\theta})\theta - G(\theta)) \tag{46}$$

The joint angle error, velocity error, and acceleration error are defined as $e = \theta_d - \theta, \dot{e} = \dot{\theta}_d - \dot{\theta}, \ddot{e} = \ddot{\theta}_d - \ddot{\theta}$ respectively. The control law u becomes

$$u = \ddot{\theta}_d + 2\lambda e + \lambda^2 \dot{e} \tag{47}$$

where $\lambda > 0$ leads to an exponentially stable closed-loop system. The closed-loop error dynamics can be derived from Eq. (46) and (47) as [32]

$$\ddot{e} + 2\lambda\dot{e} + \lambda^2 e = 0 \tag{48}$$

The SCARA robot closed-loop control model is shown below

$$M(\theta)u + V(\theta, \dot{\theta})\dot{\theta} + G(\theta) = \tau \tag{49}$$

This closed-loop control algorithm (Eq. (49)) is called the computed torque method. PD control is introduced in the closed-loop control model (Eq. (49)), the control law u is defined as

$$u = \ddot{\theta}_d + K_P e + K_d \dot{e} \tag{50}$$

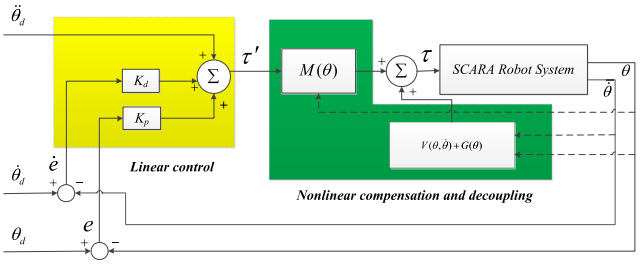

FIGURE 4. Decoupling control structure diagram.

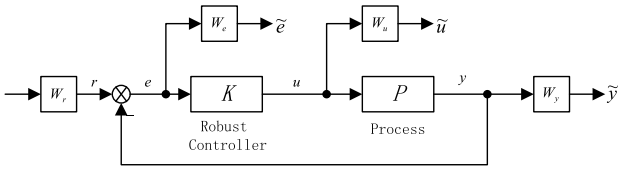

FIGURE 5. Robust control structure diagram.

where, $K_P = diag[K_{P1}, K_{P2}, K_{P3}]$ and $K_d = diag[K_{d1}, K_{d2}, K_{d3}]$ are matrices of position and velocity gains, respectively (see Fig. 5.). The PD feedback controller can be obtained by substituting Eq. (50) into Eq. (49) and then

$$M(\theta)(\ddot{\theta}_d + K_p e + K_d \dot{e}) + V(\theta, \dot{\theta})\dot{\theta} + G(\theta) = \tau \tag{51}$$

The block diagram (Fig. 4.) shows two feedback loops: internal loop based on robot dynamics model and outer loop based on tracking error. The internal loop is intended to obtain a linear and decoupled input-output relationship, while the outer loop is to stabilize the entire system. Since the outer loop is a linear stationary system, the controller design can be simplified. The stability of the control algorithm is very important for any mechanical system. In [33], A Lyapunov function is constructed and the above control algorithm is proved to have global asymptotic stability.

B. ROBUST CONTROL OF THE DECOUPLED SYSTEM

The PD controllers used in above session are simple. However, many uncertainties still exist because of mismatching of the model parameters, frictions and disturbances. Robust control is based on a nonlinear model with uncertainty to analyze the system and design the controller. Therefore robust control theory is looked as a worst-case analysis method rather than a typical case method. It is thus a good choice for the complicated system like SCARA robot with many uncertainties and high frequency resonances [34]. The H_∞ control problem in practice can be transformed into the standard H_∞ control problem, as shown in Fig. 5.

Where, $w \in R^l$ is the input signal, $u \in R^n$ is the control signal, $y \in R^m$ is the measurement feedback signal, and $z \in R^p$ is the control output signal. According to the dimensions of w, z, u and y, the $G(s)$ can be derived. From Fig. 6, the control

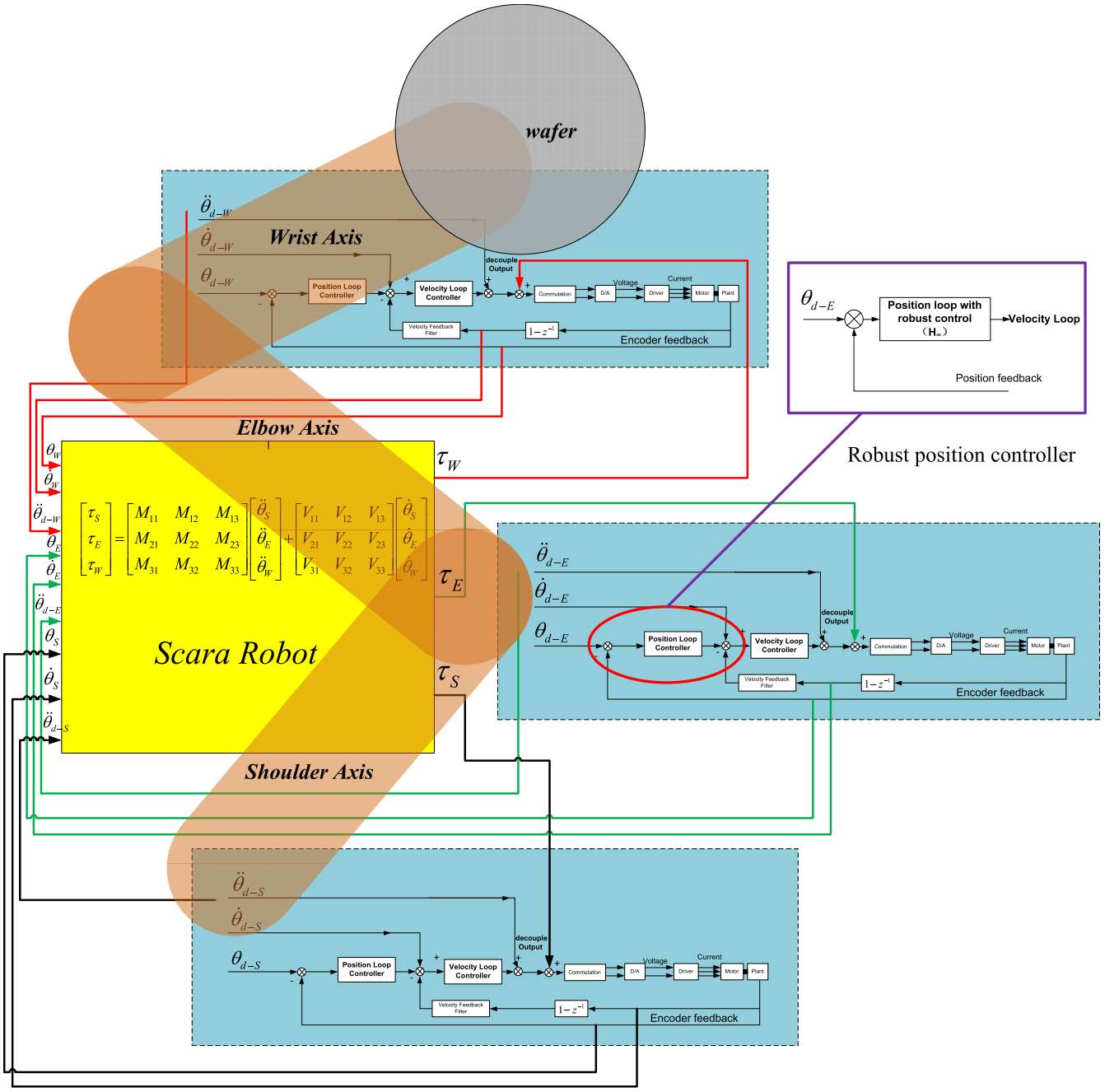

FIGURE 6. SCARA MIMO Decoupling Control and Servo Control Structure.

system can be written as

$$\begin{cases} \begin{bmatrix} z(s) \\ y(s) \end{bmatrix} = G(s) \begin{bmatrix} w(s) \\ u(s) \end{bmatrix} = \begin{bmatrix} G_{11}(s) & G_{12}(s) \\ G_{21}(s) & G_{22}(s) \end{bmatrix} \begin{bmatrix} w(s) \\ u(s) \end{bmatrix} \\ u(s) = K(s)y(s) \end{cases} \tag{52}$$

where, $G_{11}(s) \in R^{p\times l}(s), G_{12}(s) \in R^{p\times n}(s), G_{21}(s) \in R^{m\times l}(s), G_{22}(s) \in R^{m\times n}(s)$. From Eq. (52), the transfer function between w and z becomes

$$z(s) = F_l(G(s), K(s))\omega(s) \tag{53}$$

$$F_l(G(s), K(s)) = T_{zw}(s) = G_{11}(s) + G_{12}(s)K(s) \times [I_m - G_{22}(s)K(s)]^{-1} G_{21}(s) \tag{54}$$

where, $T_{zw}(s)$ is the transfer function matrix from $w(s)$ to $z(s)$, I_m is the unit matrix. The feedback controller $k(s)$ makes the closed-loop control system stable and the sub-optimal stabilized controller satisfies the below weighting equation:

$$\|T_{zw}(s)\|_\infty < \gamma (0 < \gamma \in R) \tag{55}$$

In order to achieve an effective H_∞ controller, a coefficient γ is introduced to trade off more on performance. This idea can be explained more clear that performance is sacrificed

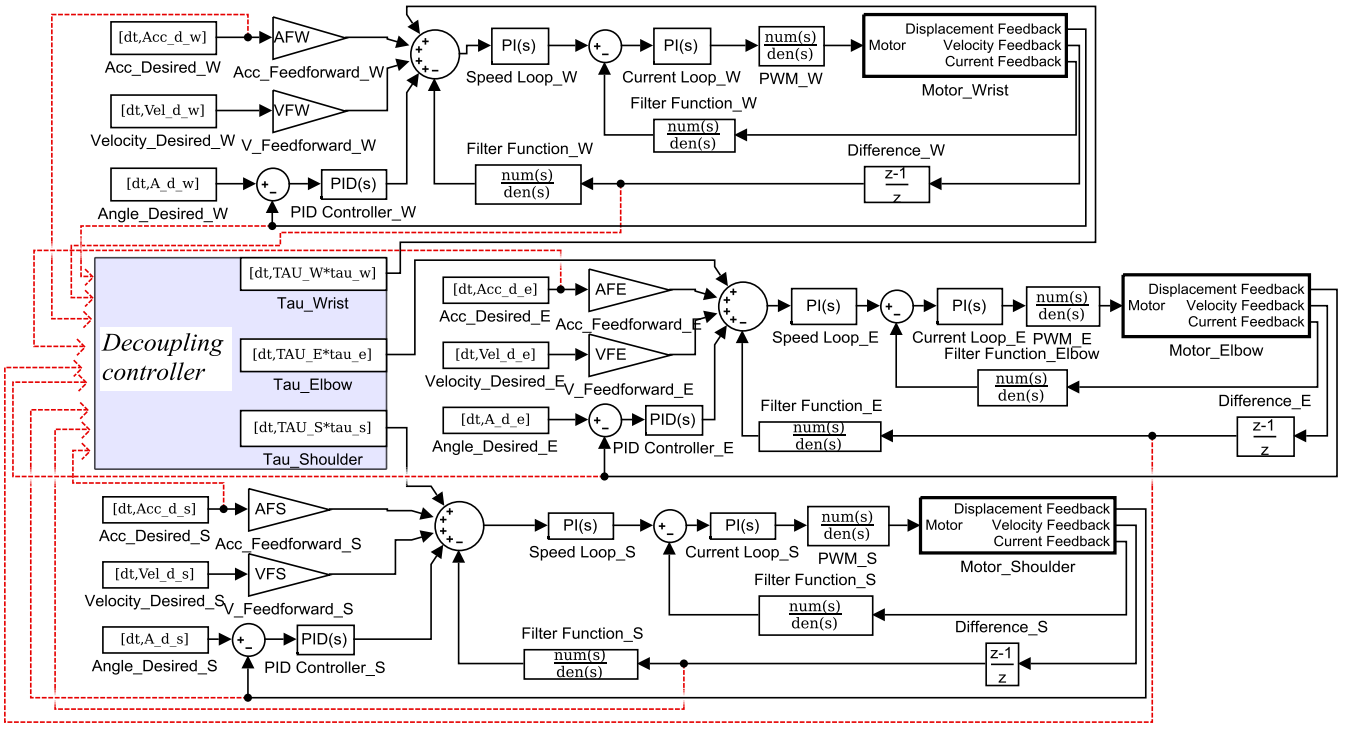

FIGURE 7. Simulation model of the SCARA with decoupling controller.

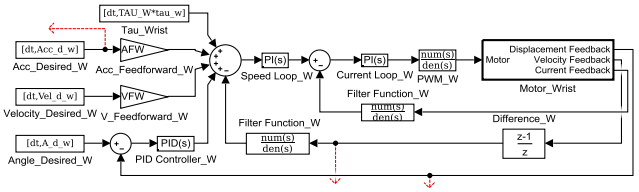

FIGURE 8. Simulation model of the Shoulder.

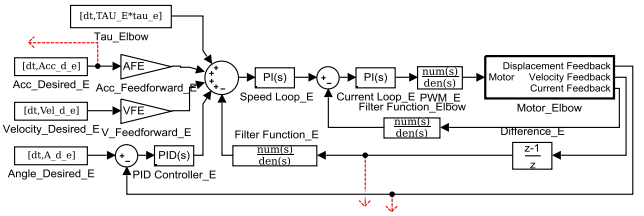

FIGURE 9. Simulation model of the Elbow.

to ensure that there exists a H_∞ controller, which is stable, unsaturated, and robust as requested. And through tuning γ, we may expect to acquire the ideal gain of SCARA robot H_∞ controller at low frequencies. Fig. 6 shows the SCARA MIMO decoupling control and the servo control structure.

In this system, robust controllers solve interference problems. The decoupling controller solves the nonlinear problem.

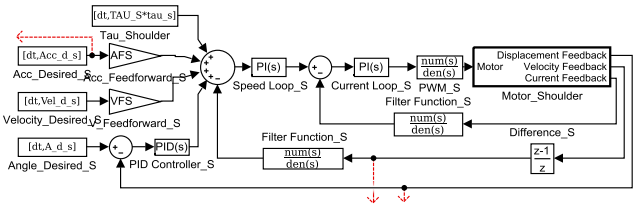

FIGURE 10. Simulation model of the Wrist.

IV. SIMULINK MODELS OF SCARA

Dynamics of the SCARA robot and decoupling controller are modeled in MATLAB Simulink environment. The Simulation model is shown in Fig. 7. Because the high frequent dynamics cause the motor to make noise, a low pass filter is added. Because this signal contains the low frequent acceleration profile, this data is smoothened and then subtracted from the original data. A movement from folded configuration to extended configuration can be considered as the most critical since at the final stage the decoupling effect and inertia plays a large role.

The Simulation model of the Shoulder, Elbow and Wrist is shown in Fig. 8, 9, and 10, respectively. The Simulation models of Shoulder, Elbow and Wrist have different independent dynamic variables. The simulation packages allow independent simulation variables. The control coefficients are illustrated in Table 2.

The decoupling and non-decoupling link angle errors of the Shoulder, Elbow and Wrist are given in Fig. 11, 12 and 13, respectively. The maximum angle errors by decoupling control are about 0.1 rad for the Shoulder, 0.001 rad for the Elbow and 0.007 rad for the Wrist.

TABLE 2. The Simulation model parameters and their values.

Parameter	Meaning	Value
PID_P_S	Proportion of PID in Shoulder	100
PID_P_E	Proportion of PID in Elbow	100
PID_P_W	Proportion of PID in Wrist	100
PID_I_S	Integral of PID in Shoulder	10
PID_I_E	Integral of PID in Elbow	10
PID_I_W	Integral of PID in Wrist	10
PID_D_S	Derivative of PID in Shoulder	10
PID_D_E	Derivative of PID in Elbow	10
PID_D_W	Derivative of PID in Wrist	10
S_L_P_S	Proportion of Speed Loop in Shoulder	80
S_L_P_E	Proportion of Speed Loop in Elbow	80
S_L_P_W	Proportion of Speed Loop in Wrist	80
S_L_I_S	Integral of Speed Loop in Shoulder	10
S_L_I_E	Integral of Speed Loop in Elbow	10
S_L_I_W	Integral of Speed Loop in Wrist	10
C_L_P_S	Proportion of Speed Loop in Shoulder	10
C_L_P_E	Proportion of Speed Loop in Elbow	10
C_L_P_W	Proportion of Speed Loop in Wrist	10
C_L_I_S	Integral of Speed Loop in Shoulder	500
C_L_I_E	Integral of Speed Loop in Elbow	500
C_L_I_W	Integral of Speed Loop in Wrist	500

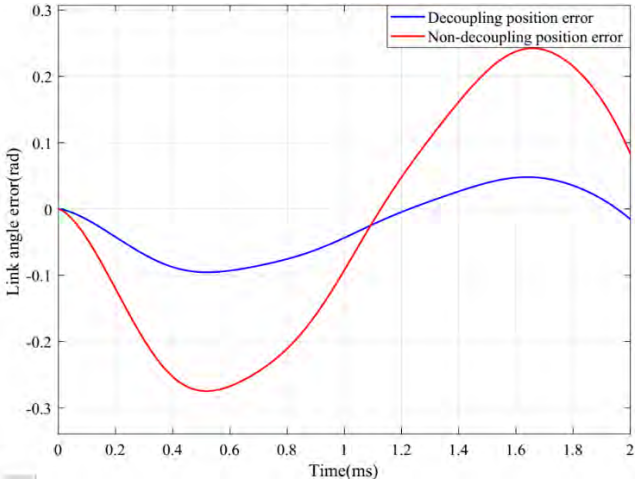

FIGURE 11. Decoupling and non-decoupling angle error of the Shoulder.

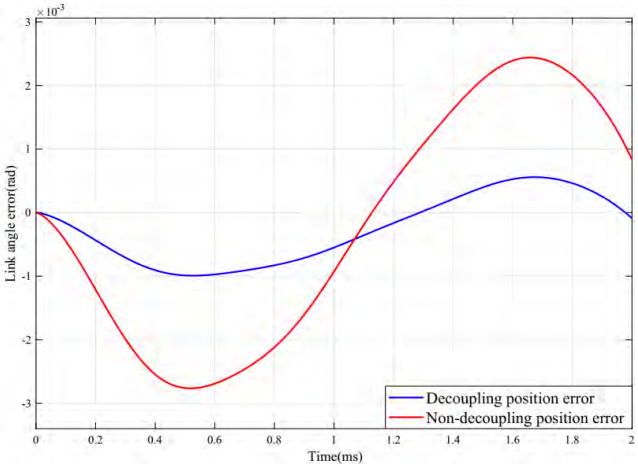

FIGURE 12. Decoupling and non-decoupling angle error of the Elbow.

V. EXPERIMENTAL RESULTS

Parameters of the SCARA robot (Fig. 14) are listed in Table 3. Three optical encoders are attached to each Direct-drive motor with 4 × 106 counts per rotation and the sampling frequency is set to 4 kHz. Fig. 15 shows SCARA robot performance comparisons with decoupling and with no decoupling control when shoulder move from 0 to 180 degree, as well

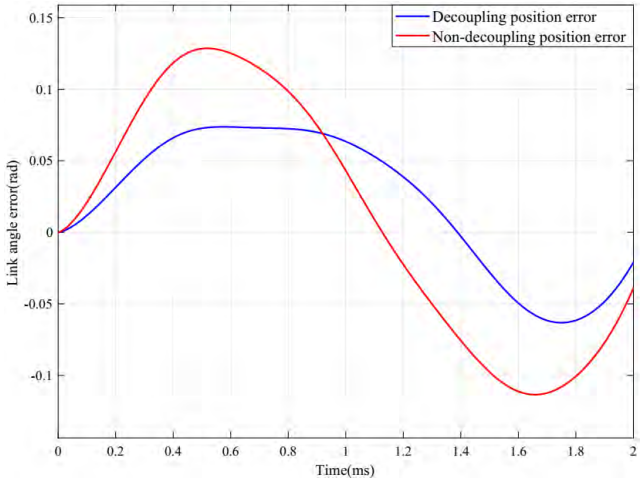

FIGURE 13. Decoupling and non-decoupling angle error of the Wrist.

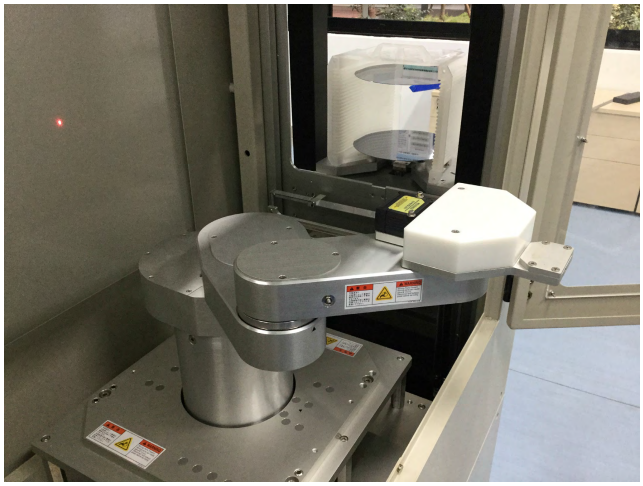

FIGURE 14. The direct-drive SCARA wafer handling robot.

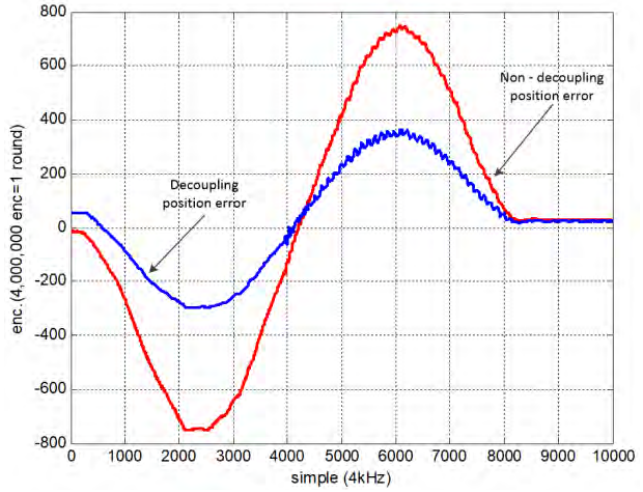

FIGURE 15. Decoupling control performance of the Shoulder axis.

TABLE 3. SCARA robot parameters and their values.

Axis	R_i	L_i	I_i	m_i
Shoulder(Axis1)	0.25m	0.073m	0.065Kg·m^2	6.32Kg
Elbow(Axis2)	0.25m	0.090m	0.056Kg·m^2	5.51Kg
Wrist(Axis3)	0.25m	0.110m	0.011Kg·m^2	1.37Kg

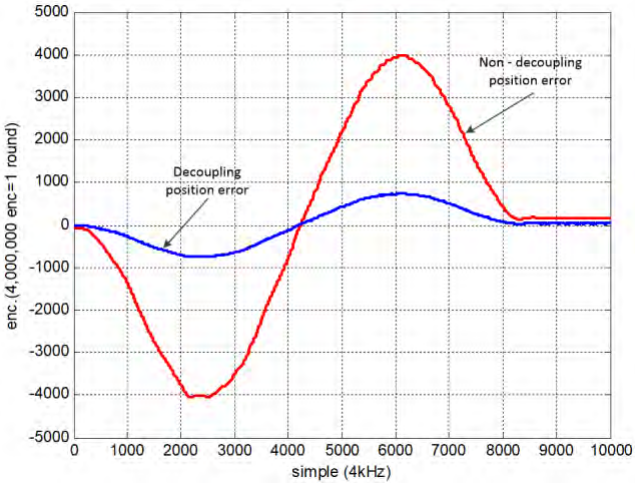

FIGURE 16. Decoupling control performance of the Elbow axis.

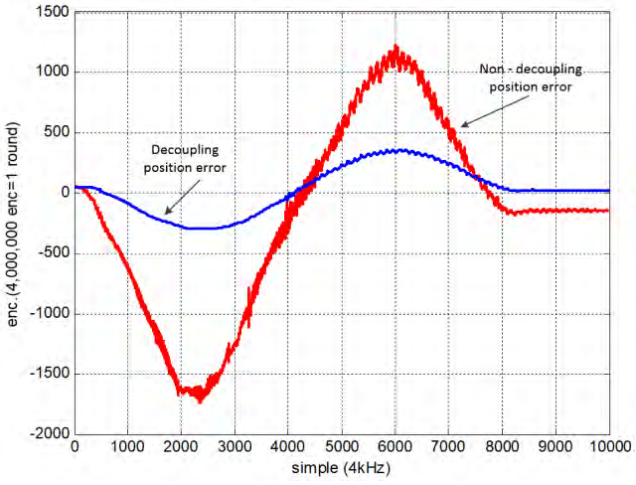

FIGURE 17. Decoupling control performance of the Wrist axis.

as wrist and elbow axes. Fig. 15 shows that the decoupling control algorithm improves a lot the position tracking accuracy of the manipulator by improving the dynamic motion performance and reducing the static tracking error.

As can be seen from Fig. 15, 16, and 17 the decoupling control algorithm and the no decoupling controller in about two seconds can make the SCARA robot system to reach a steady state, and the response speed roughly equal. Further analysis, by using the decoupling control algorithm, the three-axis overshoot of the SCARA robot is significantly reduced. Especially the elbow axis, compared with no decoupling controller, the use of decoupling control algorithm can reduce the position error by as much as 20 times. The shoulder axis and wrist axis position error is also roughly reduced by 4 to 8 times.

VI. CONCLUSION

In order to meet the high speed and high precision requirements in the process of wafer handling, this paper proposes a 4-DOF direct-drive SCARA robot. Based on coupling structure of the SCARA robot, the PD control coupled together with robust control and the feedback decoupling linearization control algorithm are presented and the corresponding controller and servo structure are designed. Through above control algorithm, the SEW (Shoulder, Elbow, Wrist axes) decoupling servo control is achieved. The experimental data shows, by comparing to non-decoupling control, decoupling control algorithm makes SCARA robot performance improved a lot. The position errors during dynamic tracking movement and the static errors are reduced by 4 to 20 times.

REFERENCES

[1] D. Cui and M. Cong, "Wafer-handling robots and applications," *Recent Patents Eng.*, vol. 3, no. 3, pp. 170–177, Nov. 2009.

[2] M. Cong, X. Yu, B. Shen, and J. Liu, "Research on a novel R-θ wafer-handling robot," in *Proc. IEEE Int. Conf. Automat. Logistics*, Aug. 2007, pp. 597–602.

[3] P. V. S. Subhashini, N. V. S. Raju, and G. V. Rao, "Parametric optimization of link lengths of a SCARA robot for deburring of circular paths," in *Proc. CAD/CAM, Robot. Factories Future*, 2016, pp. 127–135.

[4] Y. Oniz and O. Kaynak, "Control of a direct drive robot using fuzzy spiking neural networks with variable structure systems-based learning algorithm," *Neurocomputing*, vol. 149, pp. 690–699, Feb. 2015.

[5] J. Chi, H. Yu, and J. Yu, "Hybrid tracking control of 2-DOF SCARA robot via port-controlled hamiltonian and backstepping," *IEEE Access*, vol. 6, pp. 17354–17360, 2018.

[6] A. R. Moreno and V. J. Sandoval, "Fractional order PD and PID position control of an angular manipulator of 3DOF," in *Proc. Latin Amer. Robot. Symp. Competition*, Oct. 2013, pp. 89–94.

[7] S. Shu, H. Zhao, J. Yan, and B. Xi, "Research on control of two link flexible joint manipulators with improved PID method," in *Proc. 6th Int. Conf. Intell. Hum.-Mach. Syst. Cybern.*, Aug. 2014, pp. 121–124.

[8] P. R. Ouyang, V. Pano, and T. Dam, "PID position domain control for contour tracking," *Int. J. Syst. Sci.*, vol. 46, no. 1, pp. 111–124, Jan. 2015.

[9] M. R. Soltanpour, P. Otadolajam, and M. H. Khooban, "Robust control strategy for electrically driven robot manipulators: Adaptive fuzzy sliding mode," *IET Sci., Meas. Technol.*, vol. 9, no. 3, pp. 322–334, May 2015.

[10] L. Boutat-Baddas, H. S. Ali, and M. Darouach, "State estimation of a SCARA Robot using sliding mode observers," in *Proc. Eur. Control Conf.*, Jul. 2015, pp. 1836–1841.

[11] F. A. Bouaziz, Y. Bouteraa, and N. Derbel, "Control energy comparison between 1st and 2nd order sliding mode approach with application to a SCARA robot," in *Proc. 13th Int. Multi-Conf. Syst., Signals Devices*, Mar. 2016, pp. 757–761.

[12] M. R. Safanah and M. M. Shaymaa, "Improved trajectory tracking control for a three axis SCARA robot using fuzzy logic," *IRAQI J. Comput., Commun. Control Syst. Eng.*, vol. 16, no. 1, pp. 11–19, 2016.

[13] K. Lochan and B. K. Roy, "Control of two-link 2-DOF robot manipulator using fuzzy logic techniques: A review" in *Proc. 4th Int. Conf. Soft Comput. Problem Solving*, vol. 335, Dec. 2015, pp. 499–511.

[14] H. Delavari, R. Ghaderi, N. A. Ranjbar, S. H. HosseinNia, and S. Momani, "Adaptive fractional PID controller for robot manipulator," in *Proc. 4th IFAC Workshop Fractional Differentiation Appl.*, Oct. 2010, pp. 1–7.

[15] R. Mosalanezhad and M. Pourahmadi, "A novel hybrid method to adaptive robust control of an industrial four degrees of freedom SCARA robot," *J. Comput. Theor. Nanosci.*, vol. 13, no. 1, pp. 130–134, Jan. 2016.

[16] H. Zhou, H. Ma, M. Fu, Y. Lei, and H. Zhan, "Sampled adaptive control for multi-joint robotic manipulator with force uncertainties," in *Proc. Int. Conf. Intell. Robot. Appl. (ICIRA)*, vol. 9834, Aug. 2016, pp. 14–25.

[17] R. Y. Putra *et al.*, "Neural network implementation for invers kinematic model of arm drawing robot," in *Proc. Int. Symp. Electron. Smart Devices*, Nov. 2016, pp. 153–157.
[18] J. Narayan and A. Singla, "ANFIS based kinematic analysis of a 4-DOFs SCARA robot," in *Proc. 4th Int. Conf. Signal Process., Comput. Control*, Sep. 2017, pp. 205–211.
[19] E. A. H. Sallam and W. M. F. Abouzaid, "NXT∗ SCARA model based on an adaptive neural network controller," *Artif. Intell. Syst. Mach. Learn.*, vol. 7, no. 2, pp. 1818–1869, Feb. 2016.
[20] N. Nikdel, M. A. Badamchizadeh, V. Azimirad, and M. A. Nazari, "Adaptive backstepping control for an n-degree of freedom robotic manipulator based on combined state augmentation," *Robot. Comput.-Integr. Manuf.*, vol. 44, pp. 129–143, Apr. 2017.
[21] L. Zouari, H. Abid, and M. Abid, "Backstepping controller for electrically driven flexible joint manipulator under uncertainties," *Int. J. Appl. Eng. Res.*, vol. 10, no. 8, pp. 19885–19896, Jan. 2015.
[22] H. M. Kim, C. D. Lee, D. H. Kim, and K. T. Park, "Impedance control of robot manipulator using artificial intelligence," in *Proc. ICCAS*, Oct. 2010, pp. 1891–1894.
[23] N. N. Son, C. V. Kien, and H. P. H. Anh, "A novel adaptive feed-forward-PID controller of a SCARA parallel robot using pneumatic artificial muscle actuator based on neural network and modified differential evolution algorithm," *Robot. Auton. Syst.*, vol. 96, pp. 65–80, Oct. 2017.
[24] M. M. Fateh and S. Fateh, "Fine-tuning fuzzy control of robots," *J. Intell. Fuzzy Syst.*, vol. 25, no. 4, pp. 977–987, Oct. 2013.
[25] F. G. Rossomando and C. M. Soria, "Discrete-time sliding mode neuro-adaptive controller for SCARA robot arm," *Neural Comput. Appl.*, vol. 28, no. 12, pp. 3837–3850, Dec. 2017.
[26] R. Wang, Y. Qiao, and T. Lv, "Movement decoupling control for two-axis fast steering mirror," in *Proc. 2nd Int. Conf. Photon. Opt. Eng.*, Feb. 2017, vol. 10256, no. 1, pp. 10–25.
[27] L. Zhang, J. Zuo, X. Zhang, X. Yao, and L. Shuai, "A new approach to inverse kinematic solution for a partially decoupled robot," in *Proc. Int. Conf. Control, Automat. Robot.*, May 2015, pp. 55–59.
[28] M. Ali and L. Mehennaoui, "Active disturbance rejection control of a SCARA robot arm," *Int. J. U-E-Service, Sci. Technol.*, vol. 8, no. 1, pp. 435–446, 2015.
[29] M. Wilson and M. W. Spong, "Dynamics," in *Robot Modeling and Control*, 1st ed. New York, NY, USA: Wiley, 2006, pp. 187–225.
[30] C. Zhao and L. Guo, "PID controller design for second order nonlinear uncertain systems," *Sci. China-Inf. Sci.*, vol. 60, no. 2, Feb. 2017, Art. no. 022201.
[31] F. Fahimi, *Autonomous Robots*, Berlin, Germany: Springer, vol. 34, no. 2, pp. 102–115, Feb. 2018.
[32] H. M. Al-Qahtani, A. A. Mohammed, and M. Sunar, "Dynamics and control of a robotic arm having four links," *Arabian J. Sci. Eng.*, vol. 42, no. 5, pp. 1841–1852, May 2017.
[33] J. J. Craig, "Velocity kinematics," in *Introduction to Robot Mechanics and Control*, vol. 3, 2nd ed. New York, NY, USA: Addison-Wesley Co, 1989, ch. 4, Sec. 3, pp. 125–126.
[34] C. Zhang, G. Zhao, and K. J. Tseng, "Robust decoupling control of a three-link robot arm directly driven by permanent magnet synchronous motors," *Int. J. Appl. Electromagn. Mech.*, vol. 36, no. 4, pp. 279–293, Jul. 2011.

YUNBO HE received the Ph.D. degree from Xi'an Jiaotong University. He was a Postdoctoral Fellow with Nanyang Technological University, Singapore, from 2000 to 2002.

He was a Technical Manager with ASM Technology Singapore Pte., Ltd., from 2002 to 2010, and a General Manager and the Chief Engineer with Hans Photoelectric Equipment Co., Ltd., from 2010 to 2015. He currently serves as a Professor with the MOE Key Laboratory of Electronic Manufacturing Equipment, Guangdong University of Technology. His research interests include motion control, semiconductor packaging equipment, and industrial SCARA robots.

XIQUAN MAI was born in Shunde, China, in 1996. He is currently pursuing the B.S. degree with the School of Electromechanical Engineering, Guangdong University of Technology, Guangzhou, China.

His research interests include motion control, semiconductor packaging equipment, industrial SCARA robots, automation, and machine intelligence. He has authored two peer-reviewed papers and holds over ten patents.

Mr. Mai was a recipient of the China National Scholarship and the Mathematical Contest in Modeling Prize (MCM).

CHENGQIANG CUI received the Ph.D. degree in electrochemical engineering from the University of Essex, U.K., in 1991.

He has more than 20 years of experience in microelectronics research, integrated circuit packaging, high density packaging substrate development, and production experience. He is currently a Professor and a Ph.D. Supervisor with the Guangdong University of Technology (GDUT), Guangzhou, China. He has applied for nearly 100 patents and published more than 120 journal and conference papers. He is a member of the Technical Committee of the International Conference on Electronic Packaging Technology (ICEPT).

JIAN GAO received the M.Sc. degree from the Huazhong University of Science and Technology, Wuhan, China, in 1993, and the Ph.D. degree in materials, mechanical, and manufacturing engineering from the University of Nottingham, Nottingham, U.K., in 2002, where she was a Postdoctoral Research Fellow with the School of Materials, Mechanical and Manufacturing Engineering, from 2002 to 2004.

She is currently a Professor with the School of Electromechanical Engineering, Guangdong University of Technology, Guangzhou, China. Her research interests include semiconductor packaging equipment technology, digital manufacturing, and remanufacturing engineering.

ZHIJUN YANG received the B.S. degree in mechatronics engineering and the M.S. and Ph.D. degrees in solid mechanics from Jilin University, China, in 2000, 2003, and 2006, respectively.

He is currently a Professor with the School of Electromechanical Engineering, Guangdong University of Technology, Guangzhou, China. His research interests include structural multidisciplinary optimization, motion control, semiconductor manufacturing equipment, and compliant mechanism.

KAI ZHANG received the Ph.D. degree in mechanical engineering from The Hong Kong University of Science and Technology, Hong Kong, in 2008.

She is currently a Professor with the School of Electromechanical Engineering, Guangdong University of Technology, Guangzhou, China. Her research interests include microelectronic packaging, LED packaging, thermal management design, and so on.

XUN CHEN received the B.Eng. degree (Hons.) in computer interactive and communication system engineering from the University of Birmingham, in 2010, and the Ph.D. degree from Brunel University London, in 2016.

He is currently an Associate Professor with the School of Electromechanical Engineering, Guangdong University of Technology, Guangzhou, China. His research interests include smart manufacturing, industrial 4.0 machining technologies, smart controls, robotic technologies, and related technologies.

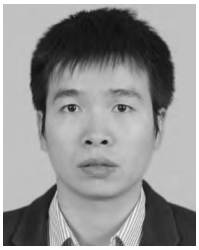

YUN CHEN received the B.S. and Ph.D. degrees in mechanical engineering from Central South University, Changsha, China, in 2009 and 2014, respectively.

He was a Visiting Scholar with the Georgia Institute of Technology, from 2016 to 2017. He is currently an Associate Professor with the School of Electromechanical Engineering, Guangdong University of Technology, Guangzhou, China, and also a Hong Kong Scholar Postdoctoral Fellow with The Chinese University of Hong Kong. He has authored more than 20 peer-reviewed papers and holds over 20 patents. His research interests include microelectronics packaging technology and equipment development.

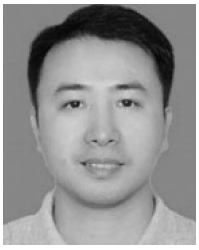

HUI TANG received the B.S. and M.S. degrees in automation and control from the Jiangxi University of Science and Technology, Guangzhou, China, in 2005 and 2008, respectively, and the Ph.D. degree in electromechanical engineering from the University of Macau, Macau, China, in 2014.

He is currently an Associate Professor with the School of Electromechanical Engineering, Guangdong University of Technology, Guangzhou, China. He has authored or coauthored 50 academic papers in journals and conferences. His research interests include flexure mechanism and nano positioning stages, semiconductor manufacturing equipment, and micro/nano device manufacturing.